

Mixed convectional and chemical reactive flow of nanofluid with slanted MHD on moving permeable stretching/shrinking sheet through nonlinear radiation, energy omission

Saleem Nasir, Sekson Sirisubtawee, Pongpol Juntharee, and Taza Gul

Citation: Chin. Phys. B, 2024, 33 (**5**): 050204. DOI: 10.1088/1674-1056/ac7dbf
Journal homepage: http://cpb.iphy.ac.cn; http://iopscience.iop.org/cpb

What follows is a list of articles you may be interested in

Couple stress and Darcy Forchheimer hybrid nanofluid flow on a vertical plate by means of double diffusion Cattaneo-Christov analysis

Hamdi Ayed
Chin. Phys. B, 2023, 32 (**4**): 040205. DOI: 10.1088/1674-1056/ac7bfb

Influences of Marangoni convection and variable magnetic field on hybrid nanofluid thin-film flow past a stretching surface

Noor Wali Khan, Arshad Khan, Muhammad Usman, Taza Gul, Abir Mouldi, and Ameni Brahmia
Chin. Phys. B, 2022, 31 (**6**): 064403. DOI: 10.1088/1674-1056/ac3a5d

Investigation of hypersonic flows through a cavity with sweepback angle in near space using the DSMC method

Guangming Guo(郭广明), Hao Chen(陈浩), Lin Zhu(朱林), and Yixiang Bian(边义祥)
Chin. Phys. B, 2021, 30 (**7**): 074701. DOI: 10.1088/1674-1056/abf7ad

Flow characteristics of supersonic gas passing through a circular micro-channel under different inflow conditions

Guang-Ming Guo(郭广明), Qin Luo(罗琴), Lin Zhu(朱林), Yi-Xiang Bian(边义祥)
Chin. Phys. B, 2019, 28 (**6**): 064702. DOI: 10.1088/1674-1056/28/6/064702

A new kind of hairpin-like vortical structure induced by cross-interaction of sinuous streaks in turbulent channel

Jian Li(李健), Gang Dong(董刚), Hui Zhang(张辉), Zhengshou Chen(陈正寿), Zhaode Zhang(张兆德)
Chin. Phys. B, 2018, 27 (**8**): 084701. DOI: 10.1088/1674-1056/27/8/084701

Mixed convectional and chemical reactive flow of nanofluid with slanted MHD on moving permeable stretching/shrinking sheet through nonlinear radiation, energy omission

Saleem Nasir[1,†], Sekson Sirisubtawee[1], Pongpol Juntharee[1], and Taza Gul[2]

[1] *Department of Mathematics, Faculty of Applied Science, King Mongkut's University of Technology North Bangkok, Bangkok* 10800, *Thailand*
[2] *Department of Mathematics, City University of Science and Information Technology, Peshawar, Pakistan*

(Received 9 May 2022; revised manuscript received 15 June 2022; accepted manuscript online 2 July 2022)

Hybrid nanofluids are remarkable functioning liquids that are intended to reduce the energy loss while maximizing the heat transmission. In the involvement of suction and nonlinear thermal radiation effects, this study attempted to explore the energy transmission features of the inclined magnetohydrodynamic (MHD) stagnation flow of CNTs-hybrid nanofluid across the nonlinear permeable stretching or shrinking sheet. This work also included some noteworthy features like chemical reactions, variable molecular diffusivity, quadratic convection, viscous dissipation, velocity slip and heat omission assessment. Employing appropriate similarity components, the model equations were modified to ODEs and computed by using the HAM technique. The impact of various relevant flow characteristics on movement, heat and concentration profiles was investigated and plotted on a graph. Considering various model factors, the significance of drag friction, heat and mass transfer rate were also computed in tabular and graphical form. This leads to the conclusion that such factors have a considerable impact on the dynamics of fluid as well as other engineering measurements of interest. Furthermore, viscous forces are dominated by increasing the values of $\lambda_{\mathrm{p}}, \delta_{\mathrm{m}}$ and δ_{q}, and as a result, $F'(\xi)$ accelerates while the opposite trend is observed for M and ϕ. The drag friction is boosted by the augmentation M, λ_{p} and ϕ, but the rate of heat transfer declined. According to our findings, hybrid nanoliquid effects dominate that of ordinary nanofluid in terms of $F'(\xi)$, $\Theta(\xi)$ and $\phi(\xi)$ profiles. The HAM and the numerical technique (shooting method) were found to be in good agreement.

Keywords: hybrid nanofluid (SWCNT+MWCNT/H_2O), velocity slip conditions, nonlinear thermal radiation, exponential stretching/shrinking sheet, inclined magnetohydrodynamic (MHD) stagnation flow

PACS: 44.15.+a, 47.27.nd, 47.15.gm **DOI:** 10.1088/1674-1056/ac7dbf

1. Introduction

With the ever-increasing trend for heat energy due to its wide range implementations in nearly every sector of science and technology, from biomedical science to engineering and just about everything else the tremendous awareness of nanotechnologies to accelerate thermal stimulation from immediate sources has attracted researchers and scientists to pursue further research and development. Improvement of energy performance can provide a competitive advantage in a variety of applications, including plasma analysis, nanoelectronics apparatus such as microchips in machines, power plants, space cooling, electricity production, and a variety of other uses. Choi[1] discovered the concept of merging nanometer-sized materials in conventional fluids. Rawat *et al.*[2] investigated the movement of two distinct nanofluids Ag/H_2O and Cu/H_2O toward a vertically positioned Riga plate. Recently, several investigations for example Xu *et al.*[3–6] and Xing *et al.*[7] have been directed on nanofluids to investigate their heat transmission characteristics. A single kind of nanoparticle may or may not have all of the perfect characteristics needed for a certain goal, it may have exceptional thermo-physical or rheological properties. Because of the several forceful uses, hybrid nanofluids are prepared to contain a variety of features, hence they are significant. A hybrid nanofluid is a special variant of nanofluid that combines two dispersed nanomaterials in a conventional fluid. As a result, if the added materials of solid nanoparticles are chosen right, they will enhance each other's favorable aspects. These type of hybrid nanofluids offer a wide range of potential uses in almost major heat exchange disciplines, such as micromachining, transport, industrial, microsystems, and pharmaceuticals. Huang *et al.*[8] developed a hybrid nanoliquid with a volume proportion of 1:2.5 (MWCNT:Al_2O_3) by manufacturing nanosized specimens of Al_2O_3/H_2O and MWCNT/H_2O nano-fluids. Hybrid nanoparticles enhance the thermal physical properties of original fluids as evidenced by extensive study in Ahmad *et al.*[9]

Thermal radiation plays a key part in the designing of a variety of modern heat transmission technologies. Radiative and nanofluid flow through a plane surface has sparked a lot of interest in both numerically and experimentally modeling. In particular, the flow across a plane surface has been extensively studied since it may be used to explain numerous engineering and industrial applications. Major industrial sectors like rockets and spacecraft as well as nuclear power stations

†Corresponding author. E-mail: saleemnasir85@gmail.com
© 2024 Chinese Physical Society and IOP Publishing Ltd

and steam turbines all depend on rate of energy exchange under radiation. Using a porous structure and a perpendicular medium, Bakier[10] scrutinized the impact of temperature radiations on force convectional movement of nanofluids. The influence of radiation on the uniform split temperature field motion with convectional surface constraints across a swing plate were examined by Ishak *et al.*[11] The considerable influence of radiant heat on MHD nanoliquids movement among two vertical spinning medium was explored by Sheikholeslami *et al.*[12] The heat transport characteristics of Casson fluid motion in a porous media over a stretching surface having MHD and radiation effect were premeditated by Mabood *et al.*[13] Yin *et al.*[14] evaluated the effect of thermal radiation and biochemical reactions on magnetohydrodynamic Sisko liquid motion across a stretched surface with heat source and motile microbes.

Stagnation flow happens when liquid comes into contact with solid surfaces. The fluid flow displayed the highest rate of energy transmission, stress (static pressure), and mass deposition near the stagnation region. Whenever fluid velocity goes to zero it produces the greatest pressure, as per Bernoulli principle. The reason for this is that the fluids kinetic energy is turned into pressure, which is termed as stagnation pressure (static pressure). Hiemenz[15] is the inventor of the fluid flow via a plane stagnation point. He employed transformation technique to translate the momentum expression into a system of nonlinear ODEs for a two-dimension stagnation flow problem on a flat sheet. Several scholars nowadays have expanded this concept to examine various characteristics of stagnation point flow problems. Because of its numerous practical applications, the concept of stagnation point flow continues to capture the interests of several scientists and scholars. Electronic device cooling, cooling of nuclear power plants during unexpected failure, fluid dynamic mechanisms in engineering disciplines, MHD power systems and cooling of unbounded metal plates in a bath, and metallurgy procedures like sketch, annealing, and tinning of copper cables are all examples of these applications.[16] Homann[17] investigated axially symmetric stagnation stream on a sphere and a cylinder. Soomro *et al.*[18] explored the role of heat absorption/generation with radiations on stagnation flow along a moving surface. Shen *et al.*[19] examined the mixed convective MHD flow closed to the stagnation point over a nonlinear starching surface. Rehman *et al.*[20] examined the nanofluid motion and energy transmission of at a stagnation on a continuously extending medium affected by the magnetization. The mathematical formulation of nanoliquid stagnation motion associated with energy and mass transport on a rolling surface with slip velocity was explored by Khashi'ie *et al.*[21] Nasir *et al.*[22] explored the effects of radiation and heat source in a 3D magnetohydrodynamics stagnation flow of engine oil based MWCNTs+Cu-hybrid nanofluid through a permeable spherical tube. Recently some other investigations such as Waini *et al.*,[23,24] may be reported in the literature to visualize the stagnation flow of fluid in different geometries under various conditions.

However, utilizing nanofluid in a permeable medium to optimize the convective heat transformation characteristics for industrial and engineering activities is also a feasible alternative. Therefore, the topic of permeable medium is receiving a lot of attention from scientists and engineers. It is because many industrial applications use this sort of infrastructure like fuel flow purification process, thermodynamical insulator, underground aquifers and heat exchangers. Furthermore, similar type of configurations is also encountered in a variety of applications such as electronics coolant apparatus, ignition processes and conditioning rotor blades, all of which involve freezing or warming mechanism. The merging of small as well as higher energy liquids has a significant influence on the working of such technologies.[25] Hassan *et al.*[26] explored the flow of liquids over a moving plate. The flow of Poiseuille nanofluid in a permeable surface involving Stefan blowing was studied by Alamri *et al.*[27] In addition, various review publications[28–30] extensively discuss nanofluid flow in porous surface.

Nanofluids and hybrid nanofluids play an important role in thermal management applications compared to the conventional fluids. The main goal of the current investigation is to examine the various characteristics of energy exchange, concentration and mobility of a hybrid nanofluid (SWCNT+MWCNT/H_2O) over a nonlinear shrinking/expanding sheet. In the present investigation, the work of Shen *et al.*[19] is further extended. The current analysis is unique because it investigates the nonlinear convectional stagnation point flow of a hybrid nanofluid. Secondly, the impact of suction/injection and nonlinear radiation is seriously contemplated. Furthermore, the impacts of the porous media, chemical reactions, varying molecular diffusivity, viscous dissipation, velocity slip and heat omission are taken into account. The inclusion of angled MHD in the flow zone is more significant in maintaining the dynamic characteristic. Therefore, the present work is intended to fill that hole. So, this paper is designed to fill this void. The findings of essential model factors on velocity, temperature, concentration, drag friction, heat and mass transfer rate are discussed by using a variety of graphs and tables. This proposed model will be used in a variety of domains, including meteorological exploration, biochemical technology, energy and transport development, renewable power conversions, photoelectric and biosensor microfluidics, tumbling in polymeric production, and many others sectors.

Table 1. Review of the literature to verify the model novelty.

Authors	Stagnation point	Hybrid nanoparticles	Nonlinear thermal radiation	Quadratic convection	Chemical reaction
Yin *et al.*[14]	✓	×	×	×	×
Shen *et al.*[19]	✓	×	×	×	×
Waini *et al.*[24]	✓	×	×	×	×
Present	✓	✓	✓	✓	✓

2. Model formulation

Under the effect of an inclined MHD, we considered the time independent 2D flow and energy transmission of a viscous, incompressible and electrically conducting hybrid nanofluid through a highly permeable nonlinearly contracting and expanding surface. Figure 1 depicts the flow analysis and coordinate axis visually. The below flow assumption is considered for the modeling of the current problem.

(i) The flow is under the effect of inclined magnetic field to sheet of strength B_0.

(ii) The shrink/stretch velocity of sheet in x-direction is u_w, u_e is the flow velocity of external boundary layer and v_w is the mass flux of the wall.

(iii) T_w, T, C_w, and C are the sheet surface and ambient temperature and concentration, respectively.

(iv) The flow is created by stretching the plate with a quadratic buoyancy force.

(v) The mechanism of non-linearly thermal radiation, viscous dissipation and heat omission/absorption is included in energy equation.

(vi) The analysis are also conducted in the presence of a varying molecule diffusivity and a chemical reaction.

The following are the model equations under the above assumptions:[9,19,21]

$$\frac{\partial u}{\partial x}+\frac{\partial v}{\partial y}=0, \tag{1}$$

$$\begin{aligned} &u\frac{\partial u}{\partial x}+v\frac{\partial u}{\partial y}\\ &=u_e\frac{\mathrm{d}u_e}{\mathrm{d}x}-\left(\frac{\sigma_{\mathrm{Hbnf}}B^2\sin^2\Omega}{\rho_{\mathrm{Hbnf}}}+\frac{\upsilon_{\mathrm{Hbnf}}}{k_p}\right)(u_e-u)\\ &+\frac{\mu_{\mathrm{Hbnf}}}{\rho_{\mathrm{Hbnf}}}\frac{\partial^2 u}{\partial y^2}+g\Upsilon_c, \end{aligned} \tag{2}$$

$$\begin{aligned} &(\rho C_p)_{\mathrm{Hbnf}}\left[u\frac{\partial T}{\partial x}+v\frac{\partial T}{\partial y}\right]\\ &=\left(k_{\mathrm{Hbnf}}+\frac{16\sigma^*}{3k^*}T_\infty^3\right)\frac{\partial^2 T}{\partial y^2}+\mu_{\mathrm{Hbnf}}\left(\frac{\partial u}{\partial y}\right)^2+Q(T-T_\infty), \end{aligned} \tag{3}$$

$$u\frac{\partial C}{\partial x}+v\frac{\partial C}{\partial y}-\frac{\partial}{\partial y}\left(D_B(C)\frac{\partial}{\partial y}\right)=-k_{ch}(C-C_\infty). \tag{4}$$

Here u and v are velocities components, k_p is signified permeability of porous medium, Υ_c is nonlinear mixed convection term and stated as[33]

$$\begin{aligned} \Upsilon_c=\{&\Upsilon_0(T-T_\infty)+\Upsilon_1(T-T_\infty)^2\\ &+\Upsilon_2(C-C_\infty)+\Upsilon_3(C-C_\infty)^2\}, \end{aligned} \tag{5}$$

where (Υ_0,Υ_1), and (Υ_2,Υ_3) are coefficient of linear and nonlinear thermal and concentration expansion, respectively, g is the gravitational force, Q represents energy omission/absorption, σ^* is the Stefan Boltzmann constant, k^* is specified the coefficient of mean absorption, k_{ch} is denoted chemical reaction and D_B is variable molecular diffusivity define as[31]

$$D_B(C)=D_{B_\infty}\left(1+\kappa_1\left(\frac{C-C_\infty}{C_0-C_\infty}\right)\right), \tag{6}$$

while κ_1 is small parameter representing variable species diffusivity parameter.

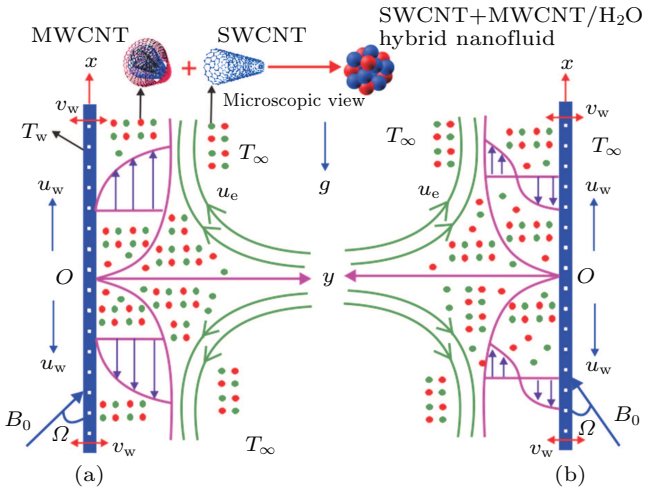


Fig. 1. Flow configuration of problem: (a) stretching case, (b) shrinking cases.

Also, σ_{Hbnf} (electrical conductivity), μ_{Hbnf} (dynamic viscosity), ρ_{Hbnf} (density), $(\rho c_p)_{\mathrm{Hbnf}}$ (capacity of specific heat) and k_{Hbnf} (thermal conductivity) are some of the hybrid nanofluid quantities described in this way,[9]

$$\begin{aligned} \frac{\mu_{\mathrm{Hbnf}}}{\mu_f}&=\frac{(1-\phi_{\mathrm{MWCNT}})^{-2.5}}{(1-\phi_{\mathrm{SWCNT}})^{2.5}},\\ \frac{\mu_{\mathrm{nf}}}{\mu_f}&=(1-\phi_{\mathrm{SWCNT}})^{-2.5},\\ \frac{\rho_{\mathrm{Hbnf}}}{\rho_f}&=(1-\phi_{\mathrm{SWCNT}})(1-\phi_{\mathrm{MWCNT}})\\ &\quad+\phi_{\mathrm{SWCNT}}(1-\phi_{\mathrm{MWCNT}})\frac{\rho_{\mathrm{MWCNT}}}{\rho_f}\\ &\quad+\phi_{\mathrm{MWCNT}}\frac{\rho_{\mathrm{SWCNT}}}{\rho_f}, \end{aligned} \tag{7}$$

$$\frac{\rho_{\mathrm{nf}}}{\rho_f}=(1-\phi_{\mathrm{SWCNT}})+\phi_{\mathrm{SWCNT}}\frac{\rho_{\mathrm{SWCNT}}}{\rho_f}, \tag{8}$$

$$\frac{(\rho c_p)_{Hbnf}}{(\rho c_p)_f} = (1-\phi_{MWCNT})(1-\phi_{SWCNT}) + (1-\phi_{MWCNT})\phi_{SWCNT}(\rho c_p)_{MWCNT} + \phi_{MWCNT}(\rho c_p)_{SWCNT},$$

$$\frac{(\rho c_p)_{nf}}{(\rho c_p)_f} = (1-\phi_{SWCNT}) + \frac{(\rho c_p)_{SWCNT}}{(\rho c_p)_f}\phi_{SWCNT}, \quad (9)$$

$$\frac{k_{Hbnf}}{k_{nf}} = (1-\phi_{MWCNT}) + 2\left(\frac{k_{SWCNT}}{k_{SWCNT}-k_{nf}}\right)k_{MWCNT}\log_e\left(\frac{k_{SWCNT}+k_{nf}}{k_{nf}}\right),$$

$$\frac{k_{nf}}{k_f} = (1-\phi_{SWCNT}) + 2\left(\frac{k_{MWCNT}}{k_{MWCNT}-k_{nf}}\right)k_{SWCNT}\log_e\left(\frac{k_{MWCNT}+k_{nf}}{k_{nf}}\right), \quad (10)$$

$$\frac{\sigma_{Hbnf}}{\sigma_f} = 1 + \frac{3\phi_{SWCNT}\sigma_{SWCNT} + 3\phi_{MWCNT}\sigma_{MWCNT} - 3\phi\sigma_f}{\sigma_f(2+\phi) + (1-\phi_{SWCNT})\sigma_{SWCNT} + (1-\phi_{MWCNT})\sigma_{MWCNT}}. \quad (11)$$

So, we assume the composition of MWCNT into SWCNT/H_2O, in the proposed investigation, a hybrid nanofluid was developed. SWCNT nanoparticles (ϕ_{SWCNT}) are firstly dispersed in H_2O to make a SWCNT/H_2O ordinary nanofluid and then MWCNT nanomaterial of diverse ratios (ϕ_{MWCNT}) are mixed to make a consistent hybrid nanofluid SWCNT+MWCNT/H_2O. We assume that $\phi = \phi_{SWCNT} + \phi_{MWCNT}$ throughout the study.

Table 2. Various thermophysical features of nanomaterials and H_2O.[9]

Features	Nanoparticles		H_2O
	SWCNT	MWCNT	
k (W/mK)	6600	3000	0.613
c_p (J/kg·K)	425	796	4179
ρ (kg/m^3)	2600	1600	997.1
σ (S/m)	10^6	10^7	5.5×10^{-6}

2.1. Boundary conditions

The corresponding physical boundary conditions of the model problem is[19]

$$\begin{aligned} &\text{at}\quad y=0,\quad u=u_w,\quad v=v_w,\quad T=T_w,\quad C=C_w,\\ &\text{at}\quad y=\infty,\quad u\to u_e,\quad T\to T_\infty,\quad C\to C_\infty, \end{aligned} \quad (12)$$

where $u_w = ax^m$, $u_e = cx^m$, $v_w = -\sqrt{a\upsilon_f}\left(\frac{m+1}{2}\right)x^{m-1/}S$, $T_w = T_\infty - T_0x^{2m-1}$, $C_w = C_\infty - C_0x^{2m-1}$ and $B = B_0x^{m-1/2}$. Here a, c, and m are constants, S is suction factor, T_0 is characteristic temperature in which opposing flow represent $T_0 > 0$ (coolant surface) while the assisting flow $T_0 < 0$ (heated surface).[19]

2.2. Corresponding transformation

To convert the above model Eqs. (1)–(4) into ODEs, we use the following equations:[19]

$$\begin{aligned} &u = cx^mF'(\xi),\\ &v = -(\nu_f c)^{\frac{1}{2}}x^{\frac{m-1}{2}}\left\{\frac{m+1}{2}F(\xi) + \frac{m-1}{2}\xi F'(\xi)\right\},\\ &\Theta(\xi) = \frac{T}{T_\infty + (T_w - T_\infty)},\\ &\phi(\xi) = \frac{C}{C_\infty + (C_w - C_\infty)}\xi = y\left(\frac{c}{\nu_f}\right)^{\frac{1}{2}}x^{\frac{m-1}{2}}, \end{aligned} \quad (13)$$

while executing the above mentioned modifications Eq. (1) is identically satisfied, whereas Eqs. (2) and (3) related with boundary restrictions (4) yield the dimensionless form shown below:[9,19]

$$N_2F''' + N_1\left(\frac{m+1}{2}FF'' - mF'^2 + m\right) + \left(N_3\sin^2\Omega M + N_2\lambda_p\right)\left(1-F'\right) + N_2\delta_m\left\{(\Theta + \delta_q\Theta^2) + \gamma_r(\phi + \gamma_q\phi^2)\right\} = 0, \quad (14)$$

$$\left(N_4 + R_d\left(1+(\Theta_w-1)\Theta\right)^3\right)\Theta'' + \Pr\left(\gamma\Theta + EcF''^2 + N_5\left(\frac{m+1}{2}F\Theta' - (2m-1)F'\Theta\right)\right) = 0, \quad (15)$$

$$(1+\kappa_1\phi)\phi'' + Sc\left(F\phi' - \frac{m+1}{2}(F'\phi') - k_r\phi\right) = 0. \quad (16)$$

The boundary constraint Eq. (12) takes the form by using Eq. (13) as

$$\begin{aligned} &F(\xi)=\lambda,\ F'(\xi)=\varepsilon,\ \Theta(\xi)=1,\ \phi(\xi)=1\ \text{at}\ \xi=0,\\ &F'(\xi)\to1,\ \Theta(\xi)\to0,\ \phi(\xi)\to0\ \text{at}\ \xi\to\infty. \end{aligned} \quad (17)$$

Here $\varepsilon = c/a$ is the extending/shrinking factor, with $\varepsilon > 0$ mentioning to the stretching case and $\varepsilon < 0$ stating to the shrinking case and $\lambda = -\left(\frac{2}{m+1}\right)\frac{v_w}{\sqrt{a\upsilon_f}}x^{\frac{m-1}{2}}$ is the constant mass flux factor with $\lambda > 0$ denoting to the suction and $\lambda < 0$ mentioning to the injection. The non-dimensional velocity, temperature and concentration components are represented by the symbols $F(\xi)$, $\Theta(\xi)$ and $\phi(\xi)$ in the preceding equations. Some constants are

$$N_1 = \frac{\rho_{Hbnf}}{\rho_f},\quad N_2 = \frac{\mu_{Hbnf}}{\mu_f},\quad N_3 = \frac{\sigma_{Hbnf}}{\sigma_f},\quad N_4 = \frac{k_{Hbnf}}{k_f},\quad N_5 = \frac{(\rho C_p)_{Hbnf}}{(\rho C_p)_f}. \quad (18)$$

Also, other non-dimensional parameters are

$$\text{Prandtl number} = Pr = \frac{\upsilon_f(\rho c_p)_f}{k_f},$$

$$\text{magnetic parameter} = M = \frac{\sigma_f B_0^2}{\rho_f a},$$

$$\text{radiation parameter} = R = \frac{4\sigma^* T_\infty^3}{k^* k_\text{f}},$$
$$\text{ckert number} = Ec = \frac{u_\text{e}}{\upsilon_\text{f}(T_\text{w} - T_\infty)},$$
$$\text{porosity factor} = \lambda_\text{p} = \frac{\upsilon_\text{f}}{k_\text{p}},$$
$$\text{mix convection factor} = \delta_\text{m} = \frac{Gr}{Re^2},$$
$$Re = \frac{x u_\text{e}}{\upsilon_\text{f}},$$
$$\text{Grashof number} = Gr = \frac{\Upsilon_0 (T_\text{w} - T_\infty) g x^3}{\upsilon_\text{f}^2},$$
$$\text{nonlinear thermal convection} = \delta_\text{q} = \frac{\Upsilon_1}{\Upsilon_0}(T_\text{w} - T_\infty),$$
$$\text{buoyancy ratio parameter} = \gamma_\text{r} = \frac{\Upsilon_2 (C_\text{w} - C_\infty)}{\Upsilon_0 (T_\text{w} - T_\infty)},$$
$$\text{nonlinear convection for concentration} = \gamma_\text{q} = \frac{\Upsilon_3}{\Upsilon_2}(C_\text{w} - C_\infty),$$
$$\text{heat source} = \gamma = \frac{Qx}{u_\text{e}(\rho c_\text{p})_\text{f}},$$
$$\text{temperature ratio factor} = \Theta_\text{w} = \frac{T_0}{T_\text{w}},$$
$$\text{chemical reaction factor} = k_\text{r} = \frac{k_\text{ch}\upsilon_\text{f}}{u_\text{e}^2},$$
$$Sc = \frac{\upsilon_\text{f}}{D_{B_\infty}}. \tag{19}$$

2.3. Physical properties of fluid

For engineering purposes, the physical values of C_f, Nu and Sh can be identified as follows:

$$C_\text{f} = \frac{1}{\rho_\text{Hbnf}}\left\{\frac{\tau_\text{w}}{u_\text{e}^2}\right\}, \quad Nu = \frac{1}{k_\text{Hbnf}}\left\{\frac{x q_\text{w}}{(T_\text{w} - T_\infty)}\right\},$$
$$Sh = \frac{1}{D_\text{B}}\left\{\frac{x q_\text{m}}{(C_\text{w} - C_\infty)}\right\}, \tag{20}$$

where τ_w, q_w and q_m are stated as

$$\tau_\text{w} = \mu_\text{Hbnf}\left(\frac{\partial u}{\partial y}\right)_{y=0},$$
$$q_\text{w} = \left(-k_\text{Hbnf}\frac{\partial T}{\partial y}\right)_{y=0} + (q_\text{r})_{y=0},$$
$$q_\text{m} = -D_B\left(\frac{\partial C}{\partial y}\right)_{y=0}. \tag{21}$$

Substituting Eq. (13) in Eq. (20), after the simplification, we obtain

$$[Re_x]^{0.5} C_\text{f} = \frac{\mu_\text{Hbnf}}{\mu_\text{f}} F''(0),$$
$$[Re_x]^{-0.5} Nu = -\left(\frac{k_\text{Hbnf}}{k_\text{f}} + R_\text{d}\left(1 + (\Theta_\text{w} - 1)\Theta\right)^3\right)\Theta'(0),$$
$$[Re_x]^{-0.5} Sh = -\phi'(0), \tag{22}$$

where $Re_x = x \cdot u_\text{w}(x)/\upsilon_\text{f}$ is the Reynolds number.

3. Solution methodology

The nonlinear boundary value problem Eqs. (14)–(17) is solved by using HAM.[32] This process commences by allowing suitable estimates and supplementary operators, which are specified as

$$F(\xi) = \lambda + 1 - \exp(-\xi), \quad \Theta(\xi) = \exp(-\xi),$$
$$\phi(\xi) = \exp(-\xi). \tag{23}$$

So, in form of linear operators, we can write

$$\Gamma_F(F) = \frac{\partial^3 F}{\partial \xi^3} - \frac{\partial F}{\partial \xi}, \quad \Gamma_\Theta(F) = \frac{\partial^2 \Theta}{\partial \xi^2} - \Theta,$$
$$\Gamma_\phi(F) = \frac{\partial^2 \phi}{\partial \xi^2} - \phi, \tag{24}$$

where the linear operators Γ_F, Γ_Θ and Γ_ϕ are

$$\Gamma_F(\dot{a}_1 + \dot{a}_2\xi + \dot{a}_3\xi) = 0,$$
$$\Gamma_\Theta(\dot{a}_4 + \dot{a}_5\xi) = 0, \quad \Gamma_\phi(\dot{a}_6 + \dot{a}_7\xi) = 0, \tag{25}$$

where the constant $\dot{a}_i$ $(i = 1, 2, \ldots, 7)$ is to be calculated.

4. Results

The goal of this research is to figure out how nonlinear radiation and convection, chemical reactions and heat source affect the energy and mass transportation factors of an inclined MHD hybrid nanofluid flow with a permeable media over a nonlinear moving surface. For various values of flow parameters such as M, λ_p, δ_m, δ_q, ϕ, Rd, Θ_w, k_r, Sc and λ, computational results of $F'(\xi)$, $\Theta(\xi)$ and $\phi(\xi)$ with the boundary layer are determined. The thermophysical properties of nanomaterials, C_f, Nu and Sh are also included in tabular and graphical form. The model physical factors are typically set from the standard source[17,19,20,24] listed as $M = \lambda_\text{p} = 0.5$, $\delta_\text{m} = 0.3 = \delta_\text{q}$, $\phi = 0.02$, $Rd = 0.4$, $\gamma = 0.2$, $\Theta_\text{w} = 1$, $k_\text{r} = 2 = Sc$, $\varepsilon = -0.2$, and $\lambda = 0.3$. The HAM technique in Mathematica software is used to compute the results of Eqs. (14)–(16), with BC in Eq. (17). We validate our findings by comparing them to the numerical method (the shooting method). The present and numerical outcomes are shown to be substantially correlated. As a result, we can confidently state that the procedure and findings of this study are accurate.

The consequence of the Mon the $F'(\xi)$ and $\Theta(\xi)$ profiles of SWCNT/H_2O (ordinary nanofluid) and SWCNT+MWCNT/H_2O (hybrid nanofluids) for shrinking surface and suction/injection situations is shown in Figs. 2(a) and 2(b), respectively. Figure 2(a) shows that increasing the value of M minimizes the liquid $F'(\xi)$ profiles in the stretching and suction/injection regimes. In general, enhancing the magnetic field produces the Lorentz force, which opposes the motion of the liquid. We demonstrated that in a stretching situation, the Lorentz force facilitates in the reduction of

fluid flow. It is worth noting that the magnetic field influence is weaker in SWCNT/H_2O nanofluid case than in the SWCNT+MWCNT/H_2O hybrid nanofluid case. The influence of the M on $\Theta(\xi)$ profile for the stretching and suction/injection conditions is revealed in Fig. 2(b). In the shrinking surface and suction/injection scenarios, boosting the M improves the $\Theta(\xi)$ for SWCNT/H_2O (ordinary nanofluid) and SWCNT+MWCNT/H_2O (hybrid nanofluids), as seen in Fig. 2(b). The basic cause for this is because when the magnitude of M grows, the width of the boundary film reduces and the thermal conductivities of the liquid strengthens. Figure 2(b) further shows that improving M elevates the $\Theta(\xi)$ profiles of the fluid in both suction and injection scenarios and it is clear that hybrid nanofluid having a greater influence than nanofluid.

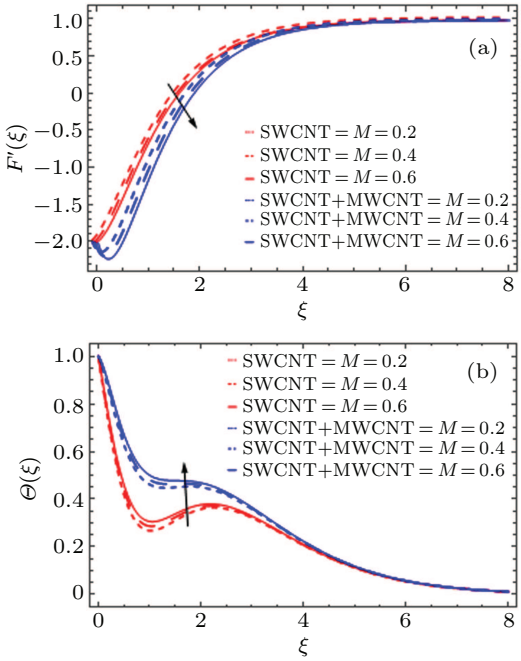


Fig. 2. Influence of M on (a) $F'(\xi)$ and (b) $\Theta(\xi)$.

Figures 3(a) and 3(b) demonstrate the influence of ϕ on $F'(\xi)$ and $\Theta(\xi)$ distribution in case of shrinking and suction. The upward variation of ϕ values depreciate the $F'(\xi)$ curves for mono and hybrid nanofluids, as seen in Fig. 3(a). The law of inverse relationship governs $F'(\xi)$ and ϕ. Physically, the addition of ϕ to the system improves the dynamic viscosity and movement diffusion mechanisms. As a result, the motion of fluid is reported to be considerably decelerated by growing value of ϕ. The $\Theta(\xi)$ profiles for both mono and hybrid nanofluids are shown in Fig. 3(b) in context of the important impact of ϕ. For $\Theta(\xi)$ and ϕ, the law of direct relation holds valid. According to the observations, the stronger impact of ϕ enables both nanofluids to demonstrate an intensification pattern. Physically, the improvement in the thermal thickness of the boundary layer and $\Theta(\xi)$ profiles is due to an increase in ϕ, which increases thermal conductivity when equated to a conventional liquid. Furthermore, because of the greater ϕ, the thermal conductivity of the hybrid nanofluid swells, allowing in a faster rate of heat transfer in response to changing $\Theta(\xi)$ profiles.

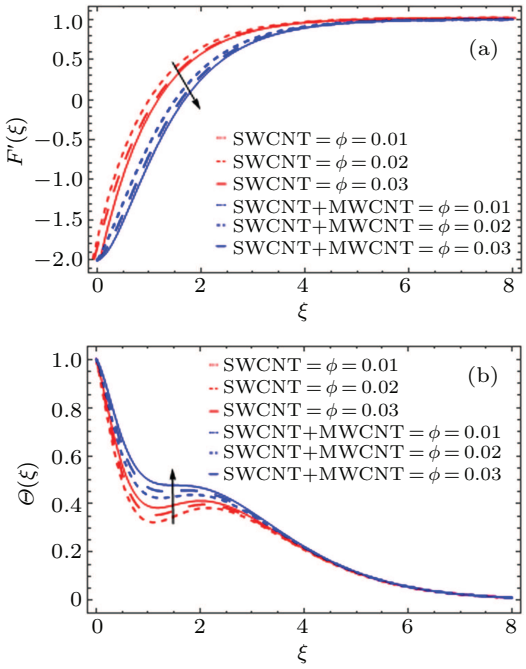


Fig. 3. Influence of ϕ on (a) $F'(\xi)$ and (b) $\Theta(\xi)$.

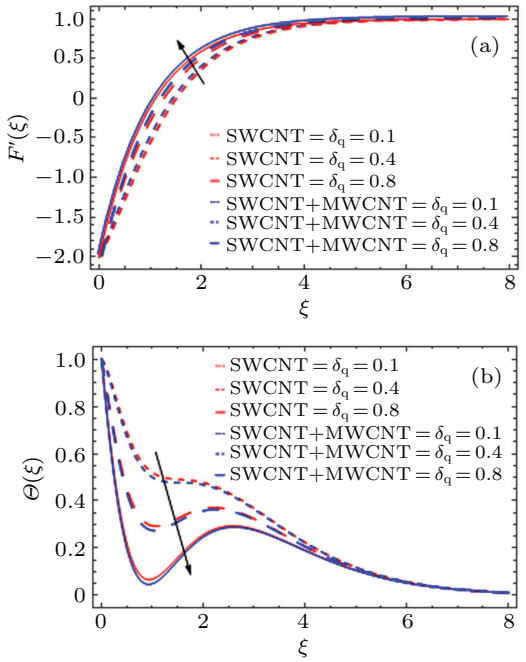


Fig. 4. Influence of δ_q on (a) $F'(\xi)$ and (b) $\Theta(\xi)$.

Figures 4(a) and 4(b) show the effect of the quadratic thermal convection parameter δ_q (nonlinear thermal convectional factor) on $F'(\xi)$ and $\Theta(\xi)$ distributions for shrinkage and suction situations. Figure 4(a) reveals that for both types of nanoliquids, the nature of $F'(\xi)$ is greater for increasing values of δ_q. Physically, the presence of δ_q factor enhances the thermal

gradient just at border of the sheet and improves the buoyancy force caused by convection, that forcing the liquid to migrate away from the sheet surface. As a result, $F'(\xi)$ is enhanced. Whereas Fig. 4(b) reveals the opposite behavior of $\Theta(\xi)$ for maximizing value of δ_q for nano and hybrid nanofluids.

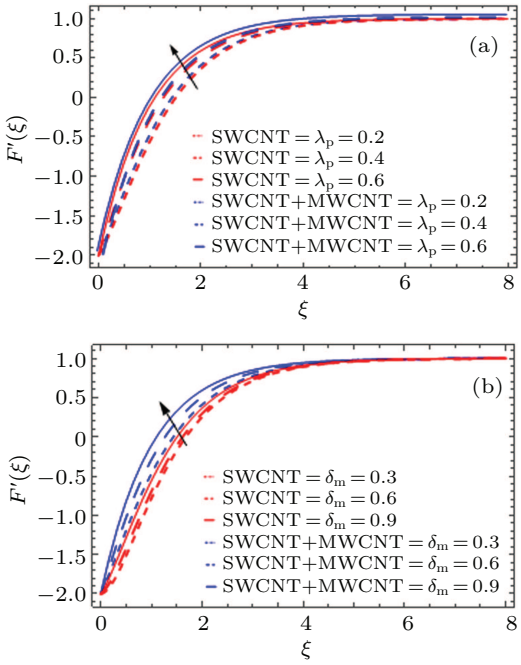


Fig. 5. Influence of (a) λ_p and (b) δ_m on $F'(\xi)$.

Figure 5(a) shows that different values of the λ_p (permeability parameter) affect the $F'(\xi)$ profile for shrinkage and suction situations. It is important to remember that boosting the porosity factor values raises the velocity curves for mono and hybrid nanoliquids. The velocity profile of the hybrid nanofluid is superior than that of a simple nanofluid. For shrinking and suction situations, the effect of δ_q (mixed convection parameter) on $\Theta(\xi)$ is depicted in Fig. 5(b). It should be emphasized that larger values of the mixed convectional factor result in an increased $\Theta(\xi)$ distribution for both mono and hybrid nanofluids. Physically, this is due to the fact that the δ_q parameter and the buoyancy force are directly proportional to each other. The thermal profile of the hybrid nanofluid is superior than that of a simple nanofluid. For various quantities of γ (temperature source parameter) and Θ_w (temperature ratio factor), numerical values of simple nanofluids and hybrid nanofluid $\Theta(\xi)$ have been computed and graphically displayed in Figs. 6(a) and 6(b). So, for both types of nanofluids, the nature of $\Theta(\xi)$ and thermal boundary layer thickness improve as γ is increased as displayed in Fig. 6(a). The thickness of the thermal boundary layers in hybrid nanofluid is superior to that of simple nanofluid. γ, which appears in the energy equation, measures the quantity of energy consumption per unit of volume. It is known as $Q_0(T_w - T_0)$, with Q_0 being energy source coefficient that could be hopeful or doubtful. The influence of the Θ_w on the $\Theta(\xi)$ field is perceived in Fig. 6(b) for nano and hybrid nanofluid. Whenever Θ_w is elevated, the $\Theta(\xi)$ profile shows a significant increase. When $\Theta_w = 1$ is taken into account, a linear thermal radiation pattern is established. Physically, a larger Θ_w indicates a significant thermal variation between the wall and the surrounding environment.

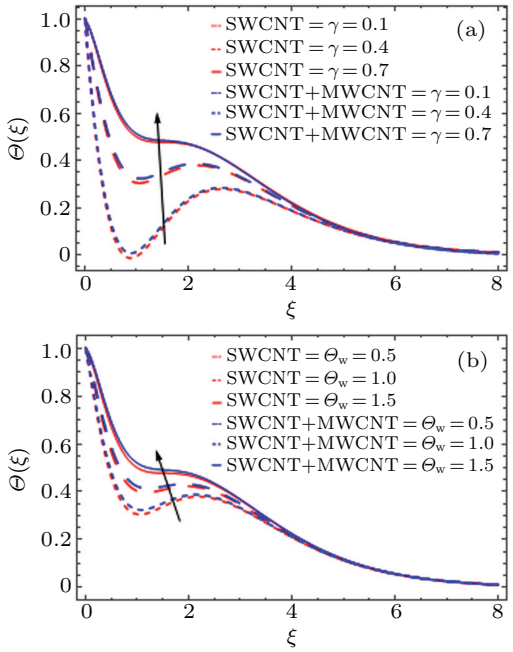


Fig. 6. Influence of (a) γ and (b) Θ_w on $\Theta(\xi)$.

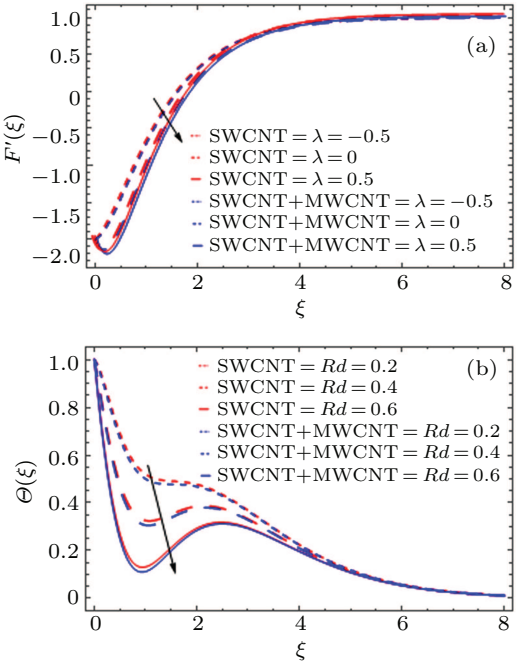


Fig. 7. Influence of (a) λ on $F'(\xi)$ and (b) Rd on $\Theta(\xi)$.

As the temperature varies, the thickness of the thermal boundary layer grows. Furthermore, hybrid nanofluid has a higher $\Theta(\xi)$ than a conventional nanofluid. We plotted Figs. 7(a) and 7(b) to highlight the influence of the λ (suction

factor) and *Rd* (radiation factor) on the nondimensional velocity $F'(\xi)$ and $\Theta(\xi)$ distribution, respectively. The graphs in Fig. 7(a) illustrate that the parameter λ has a significant impact on the width of the boundary layer. By rising λ, the flow appears to decrease significantly. Generally, suction forces the boundary layer to stick closer to the wall, destroying the momentum and causing a decrease in $F'(\xi)$. As a result of λ, the thickness of the momentum boundary layer is minimized. The influence of the *Rd* on $\Theta(\xi)$ profiles for shrinkage and suction/injection scenarios is shown in Fig. 7(b). Improvements in *Rd* cause elevations in $\Theta(\xi)$ in both circumstances of nano and hybrid nanofluids, as shown in the graphs. In the Rosseland approximation, it illustrates the dominance of radiant heat transport. Physically, the radiative portion increases the mobility of tiny molecules, forcing randomly migratory molecules to collide and the mechanical energy to be transferred into thermal energy. The $\Theta(\xi)$ profile of conventional nanofluids is slightly lower than that of hybrid nanofluids. The impact of *Sc* and k_r on $\phi(\xi)$ profiles for nano and hybrid nanofluids are shown in Figs. 8(a) and 8(b). The influence of *Sc* on the $\phi(\xi)$ field is shown in Fig. 8(a). With an increment in *Sc*, the $\phi(\xi)$ and boundary film thickness decline. This is because *Sc* is linearly proportional to the movement diffusion to the mass diffusion ratios. As a result, *Sc* represents the relative effectiveness of momentum and transportation systems by diffusion into the hydrodynamic boundary film. The drops in $\phi(\xi)$ profiles are accompanied by an unexpected decline in the thickness of the concentration boundary layer. Figure 8(b) depicts the influence of the k_r on the $\phi(\xi)$ fields. For enhancing the k_r parameter, the $\phi(\xi)$ profiles are diminished. Greater levels of k_r cause the diffusion coefficient of hybrid chemical species to drop, resulting in a reduction in $\phi(\xi)$ and boundary layer thickness. In fact, in the case of a dangerous scenario $k_r > 0$, a homogeneous chemical reaction happens after a great deal of agitation. Greater molecular mobility was created in the operating hybrid nanofluid, which improved the transportation mechanism and reduced the $\phi(\xi)$ distribution in the flow characteristics.

Figure 9(a) depicts the changes in $[Re_x]^{0.5} C_f$, and it can be seen that $[Re_x]^{0.5} C_f$ improves when the λ_p grows. The fluctuations in the $[Re_x]^{-0.5} Nu$ are shown in Fig. 9(b) and it can be seen that increasing the value of *Rd* stimulates the elevation in the $[Re_x]^{-0.5} Nu$. Similarly, the variation in $[Re_x]^{-0.5} Sh$ is shown in Fig. 9(c) and it can be seen that increasing the value of K_r stimulates the reduction in the $[Re_x]^{-0.5} Sh$.

The comparability of HAM and numerical approach for velocity, temperature, and concentration profiles is shown in Figs. 10(a), 10(b), 10(c), respectively. The analytical and numerical methodologies have a significant positive association. Tables 3, 4 and 5 show the effects of numerical values of many model variables on the $[Re_x]^{0.5} C_f$, $[Re_x]^{-0.5} Nu$ and $[Re_x]^{-0.5} Sh$ of nano and hybrids nanofluids. Table 3 presents that with greater numerical values of M, λ_p and ϕ, and $[Re_x]^{0.5} C_f$ is augmented through the wall of a shrinking or stretching sheet. Table 4 shows the $[Re_x]^{-0.5} Nu$ through the wall of a shrinking or stretching sheet when the effect of engineering factors *M*, *Rd* and ϕ are used. The $[Re_x]^{-0.5} Nu$ accelerates when *M*, *Rd* and ϕ are enhanced. Table 5 presents influence of $[Re_x]^{-0.5} Sh$ over a stretching sheet. The value of $[Re_x]^{-0.5} Sh$ improves when k_r and *Sc* are enhanced. Table 6 presents the validation of present outcomes with published results.[33,34]

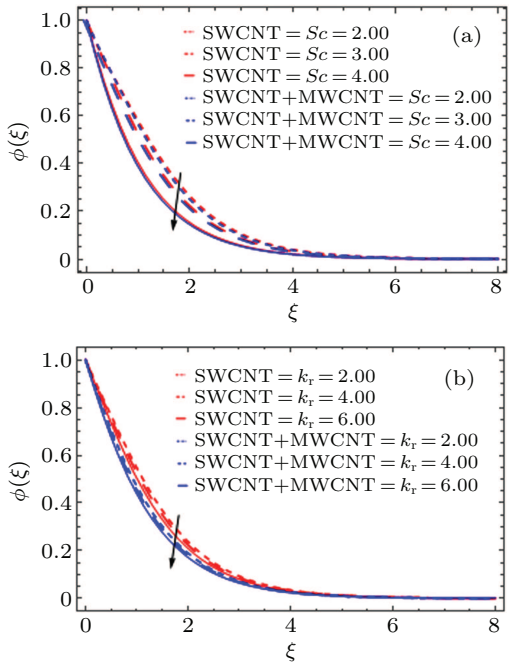


Fig. 8. Influence of (a) *Sc* and (b) k_r on $\phi(\xi)$.

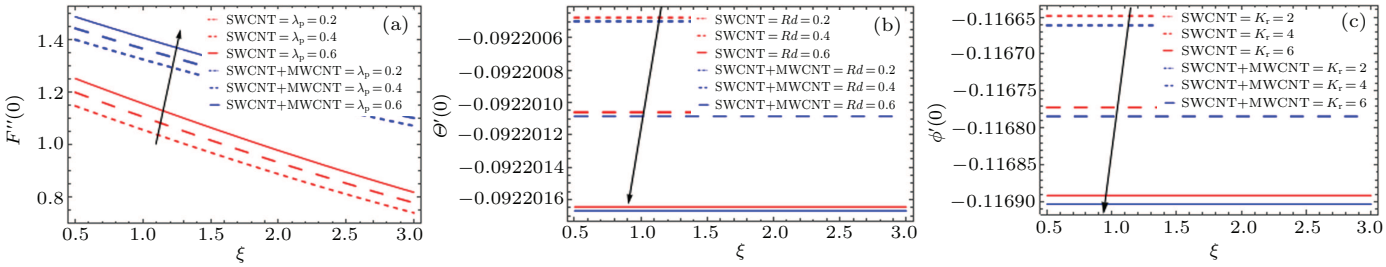


Fig. 9. Influence of (a) λ_p on $F''(\xi)$, (b) *Rd* on $\Theta'(\xi)$ and (c) K_r on $\phi'(\xi)$.

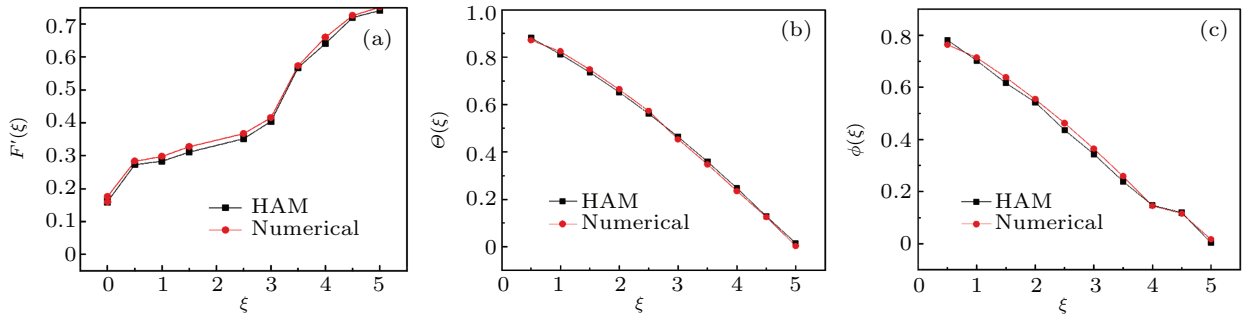


Fig. 10. Compassion graphs of HAM and numerical method for (a) $F'(\xi)$, (b) $\Theta(\xi)$ and (c) $\phi(\xi)$ with $\varepsilon = 0.15$.

Table 3. Numerical analysis of surface drag for different parameters.

M	λ_p	ϕ	$[Re_x]^{0.5} C_f$	$[Re_x]^{0.5} C_f$
			SWCNT/H_2O	SWCNT+MWCNT/H_2O
0.2	0.5	0.01	0.523456	0.56430980
0.5			0.543478	0.59087214
0.7			0.592310	0.62341590
	0.3		0.309811	0.49803225
	0.5		0.653781	0.68903217
	0.7		0.723145	0.76761341
		0.01	0.534121	0.59345178
		0.02	0.732617	0.78345187
		0.03	0.792341	0.88234510

Table 4. Numerical analysis of rate of heat transmission for different parameter.

M	Rd	ϕ	$[Re_x]^{-0.5} Nu$	$[Re_x]^{-0.5} Nu$
			SWCNT/H_2O	SWCNT+MWCNT/H_2O
0.2	0.6	0.01	0.10523782	0.15624156
0.5			0.15234719	0.19876213
0.7			0.18983415	0.21341581
	0.3		0.70923416	0.74345271
	0.6		0.72537863	0.76892314
	0.9		0.78913415	0.82341577
		0.01	0.42343412	0.51452778
		0.02	0.47323627	0.58308013
		0.03	0.52341516	0.68243599

Table 5. Numerical analysis of Sherwood number for different parameters.

k_r	Sc	$[Re_x]^{-0.5} Sh$	$[Re_x]^{-0.5} Sh$
		SWCNT/H_2O	SWCNT+MWCNT/H_2O
1.00	2.00	1.123452	1.133435
3.00		1.143345	1.151345
3.00		1.209345	1.249878
	2.00	1.612305	1.683451
	3.00	1.534256	1.592425
	4.00	1.370723	1.383001

Table 6. Estimation analysis of surface drag with previous data for different parameters.

a	m	$F''(0)$ [33]	$F''(0)$ [34]	Present
0.00	1.00	−1.000008	−1.000007	−1.000008
0.50		− −1.224780	−1.224760	−1.224775
1.00	1.00	−1.414424	−1.414421	−1.414424
0.00	3.00	−1.624355	−1.624357	−1.624356
0.50	3.00	−1.989425	−1.989423	−1.989424
1.00	3.00	−2.229718	−2.229718	−2.229718

5. Conclusion

The nonlinear convectional MHD stagnation point flow of hybrid nanofluid with the existence of nonlinear thermal radiation, chemical reactions, variable molecular diffusivity, quadratic convection, viscous dissipation and heat omission is present. The velocity slip and suction/injection conditions are imposed on the boundary of the exponentially permeable stretching/shrinking surface. The SWCNT+MWCNT/H_2O scenario for carbon nanotubes-based hybrid nanofluids are explore. The mathematical model is translated into ODE, which are then analyzed by utilizing HAM Mathematica approach. The following are the key conclusions of the paper: For both cases of SWCNT/H_2O and SWCNT+MWCNT/H_2O, higher values of M and ϕ generated a retardation effect, whereas $\Theta(\xi)$ showed the inverse correlation. The strength of viscous forces is dominated by the increasing λ_p, δ_m and δ_q, and as a result, $F'(\xi)$ accelerates for both types of nanofluids. The retardation effect occurs at larger values of M, γ and Θ_w leading to a rise in fluid $\Theta(\xi)$ for SWCNT/H_2O and SWCNT+MWCNT/H_2O. The growing magnitudes of k_r and Sc decay the concentrations, $\phi(\xi)$ profile for both nanofluids diminishes. The drag friction is boosted by the augmentation M, λ_p and ϕ. The heat transfer rate diminishes as M, Rd and ϕ are elevated. The mass transfer rate accelerates when k_r and Sc values rise.

Acknowledgement

This research was funded by King Mongkut's University of Technology North Bangkok with Contract no. KMUTNB-Post-65-07.

References

[1] Choi, S U and Eastman J A 1995 *Enhancing thermal conductivity of fluids with nanoparticles* (No. ANL/MSD/CP-84938; CONF-951135-29). Argonne National Lab., IL (United States)

[2] Rawat, S K, Mishra A and Kumar M 2019 *Multidiscipline Mod. Mater. Struct.* **15** 714

[3] Xu H and Xing Z 2017 *Int. Comm. Heat Mass Transfer.* **89** 73

[4] Xu H, Gong L, Huang S and Xu M 2015 *Int. J. Heat Mass Transfer.* **83** 399

[5] Xu H J, Xing Z B, Wang F Q and Cheng Z M 2019 *Che. Eng. Sci.* **195** 462

[6] Xu H, Xing Z and Vafai K 2019 *Int. J Heat Fluid Flow* **77** 242
[7] Xing Z B, Han X, Ke H, Zhang Q G, Zhang Z, Xu H and Wang F 2021 *Int. J Num. Methods Heat Fluid Flow* **31** 27548
[8] Huang D, Wu Z and Sunden B 2016 *Exp. Thermal Fluid Sci.* **72** 190
[9] Ahmad S, Nadeem S and Ullah N 2020 *App. Nanoscience* **10** 5107
[10] Bakier A Y 2001 *Int. Comm. Heat Mass Trans.* **28** 119
[11] Ishak A, Yacob N A and Bachok N 2011 *Meccanica* **46** 795
[12] Sheikholeslami M, Ganji D D, Javed M Y and Ellahi R 2015 *J. Magnet. Magnetic Mater.* **374** 36
[13] Mabood F, Abdel-Rahman R G and Lorenzini G 2016 *J Eng. Thermophys.* **25** 536
[14] Yin J, Zhang X, Rehman M I U and Hamid A 2022 *Case Stud. Thermal Eng.* **30** 101771
[15] Hiemen K 1911 *Dinglers Polytech. J.* **326** 324
[16] Salem A M and Fathy R 2012 *Chin. Phys. B* **21** 054701
[17] Homann F 1936 *ZAMM J App. Math. Mechan.Zeitschrift Angewandte Mathematik und Mechanik* **16** 153
[18] Soomro F A, Haq R U, Al-Mdallal Q M and Zhang Q 2018 *Results Phys.* **8** 404
[19] Shen M, Wang F and Chen H 2015 *Boundary Value Prob.* **1** 15
[20] Rehman F U, Nadeem S, Rehman H U and Haq R U 2018 *Results Phys.* **8** 316
[21] Khashi'ie N S, Md Arifin N, Nazar R, Hafidzuddin E H, Wahi N and Pop I 2019 *Energies* **12** 1
[22] Nasir S, Shah Z, Alrabaiah H, Islam S and Khan S N 2020 *Phys. Scripta* **96** 14
[23] Waini I, Ishak A and Pop I 2020 *Sci. Rep.* **10** 9296
[24] Waini I, Ishak A and Pop I 2022 *Int. Comm. Heat Mass Transfer.* **130** 105804
[25] Das S K, Choi S U S, Yu W and Pradeep T 2008 *Nanofluids: Science and Technology* (John Wiley & Sons) p. 109
[26] Hassan M, Marin M, Alsharif A and Ellahi R 2018 *Phys. Lett. A* **382** 2749
[27] Alamri S Z, Ellahi R, Shehzad N and Zeeshan A 2019 *J. Mol. Liq.* **273** 292
[28] Kasaeian A, Daneshazarian R, Mahian O, Kolsi L, Chamkha A J, Wongwises S and Pop I 2017 *Int. J. Heat Mass Transfer.* **107** 778
[29] Menni Y, Chamkha A J and Azzi A 2019 *Special Top. Rev. Porous Media* **10** 1
[30] Khanafer K and Vafai K 2019 *J. Therm. Anal. Calorimetry* **135** 1479
[31] Vajravelu K, Prasad K V, Ng C O and Vaidya H 2017 *Int. J. Mech. Mater. Eng.* **12** 1
[32] Shijun L 1998 *Appl. Math. Mech.* **19** 957
[33] Xia W F, Ahmad S, Khan M N, Ahmad H, Rehman A, Baili J and Gia T N 2022 *Case Stud. Thermal Eng.* **32** 101893
[34] Nandi S, Kumbhakar B, Seth G S, Chamkha A J 2021 *Phys. Scr.* **96** 065206